



HAL
open science

3D modeling of the Sorbas Basin (Spain): new constraints on the Messinian Erosional Surface morphology

Damien Do Couto, Charles Gumiaux, Laurent Jolivet, Romain Augier, Noémie Lebreton, Nicolas Folcher, Gwenaél Jouannic, Jean-Pierre Suc, Christian Gorini

► To cite this version:

Damien Do Couto, Charles Gumiaux, Laurent Jolivet, Romain Augier, Noémie Lebreton, et al.. 3D modeling of the Sorbas Basin (Spain): new constraints on the Messinian Erosional Surface morphology. *Marine and Petroleum Geology*, 2015, 66, pp.101-116. 10.1016/j.marpetgeo.2014.12.011 . hal-01250222

HAL Id: hal-01250222

<https://hal.science/hal-01250222>

Submitted on 4 Jan 2016

HAL is a multi-disciplinary open access archive for the deposit and dissemination of scientific research documents, whether they are published or not. The documents may come from teaching and research institutions in France or abroad, or from public or private research centers.

L'archive ouverte pluridisciplinaire **HAL**, est destinée au dépôt et à la diffusion de documents scientifiques de niveau recherche, publiés ou non, émanant des établissements d'enseignement et de recherche français ou étrangers, des laboratoires publics ou privés.

3D modeling of the Sorbas Basin (Spain): new constraints on the Messinian Erosional Surface morphology

**Damien Do Couto¹, Charles Gumiaux^{2,3,4}, Laurent Jolivet^{2,3,4}, Romain Augier^{2,3,4},
Noémie Le Bret^{2,3,4}, Nicolas Folcher⁵, Gwenaél Jouannic⁶,
Jean-Pierre Suc^{7,8}, Christian Gorini^{7,8}**

1 Earth and Environmental Sciences, University of Geneva, 1205 Genève, Switzerland

2 Université d'Orléans, ISTO, UMR 7327, 45071, Orléans, France

3 CNRS/INSU, ISTO, UMR 7327, 45071 Orléans, France

4 BRGM, ISTO, UMR 7327, BP 36009, 45060 Orléans, France

5 PPME (EA n° 3325), Université de la Nouvelle-Calédonie, BP R4 98851 Nouméa Cedex, Nouvelle-Calédonie

6 Cerema, Laboratoire de Nancy, 71 Rue de la Grande Haie, 54510 Tomblaine, France

7 Sorbonne Universités, UPMC Université Paris 6, UMR 7193, Institut des Sciences de la Terre Paris (iSTeP), 75005, Paris, France

8 CNRS, UMR 7193, Institut des Sciences de la Terre Paris (iSTeP), F-75005, Paris, France

Corresponding author: Damien Do Couto, Earth and Environmental Sciences, University of Geneva, 13 Rue des Maraîchers, 1205 Genève, Switzerland (e-mail address : damien.docouto@unige.ch)

Abstract

The scenario of the Messinian Salinity Crisis (MSC) remains one of the most debated topics in the Mediterranean realm and especially in the Sorbas Basin, which is one of the type-localities of MSC-related deposits. After a recently improved chronostratigraphic framework of the Miocene and Pliocene deposits in the basin, it appears important to image the morphology of the Messinian Erosional Surface (MES) at depth. We built a 3D model at the basin-scale of the Miocene and Pliocene series that confirms the erosional character of the Messinian/Pliocene boundary, solving a long-standing and debated question. We tentatively also suggest that the fluvial system developed during the peak of the MSC was exiting the basin toward the south. This new geometrical model, showing a robust internal consistency, can be used as a basis for interpreting the Messinian Salinity Crisis in other sedimentary basins around the Mediterranean Sea. The return of marine conditions in the Early Pliocene on an erosional surface interferes with the continuous formation of the Sorbas Basin syncline, subsidence of the hinge, uplift of the limbs and gravitational sliding. The irregular shape of the MES is superimposed by small-scale folding describing box-type folds oriented along two sub-perpendicular NE-SW and NW-SE fold axes. The architecture of these folds suggests a gravitational sliding of post-evaporitic marine sediments during the progressive deformation of the basin during the Zanclean.

1. Introduction

During the Neogene, the temporary isolation of the Mediterranean Sea caused by the successive closure of marine corridors in the region of Gibraltar induced a sudden drop of Mediterranean Sea level. This event known as the Messinian Salinity Crisis (MSC) induced the deposition of both gypsum in marginal basins and halite in the deep basin (Hsü *et al.*, 1973; CIESM, 2008). Because of its proximity to the Gibraltar area, the Alboran Sea was in a key-position to record the potential interactions between tectonics and morphological surface processes governing, in particular, Atlantic-Mediterranean water mass exchanges.

The Sorbas Basin, located in the internal zones of the Betic Cordillera (southern Spain), is a key peripheral basin where Miocene to Pliocene sediments have recorded

interactions of both tectonic and eustatic changes of the southwestern Mediterranean realm (Fig. 1). Many scenarios for the Neogene evolution of the whole Alboran region were based upon the stratigraphy and structure of the Sorbas Basin. However, several conflicting stratigraphic models of the Sorbas Basin have been published so far (Dronkert, 1976; Pagnier, 1976; Ott d'Estevou *et al.*, 1990; Riding *et al.*, 1991; Rouchy and Saint-Martin, 1992; Dabrio and Polo, 1995; Clauzon *et al.*, 1996; Conesa *et al.*, 1999; Fortuin *et al.*, 2000; Krijgsman *et al.*, 2001; Bourillot *et al.*, 2009; Roveri *et al.*, 2009; Bourillot *et al.*, 2010; Clauzon *et al.*, in revision) and while the geometries of the lower Messinian deposits have been well-established before (Weijermars *et al.*, 1985; Ott d'Estevou and Montenat, 1990), the spatial relationships between the Messinian gypsum and post-MSC deposits are much less constrained. Discrepancies concern the presence or absence of the Messinian Erosional Surface (MES) in the Sorbas Basin if any and its stratigraphic location. Indeed, it has been located either at the base of the Messinian evaporites (Riding *et al.*, 1999, 2000), or at the transition between marine and continental deposits in the upper part of the sedimentary units (Gautier *et al.*, 1994) or more recently, at the bottom of the Pliocene deltaic sediments (Clauzon *et al.*, in revision).

In order to better constrain the effect of the Messinian erosional period on sediments structures and of the gypsum layers on subsequent shortening through the study area, a 3D structural modeling of the Sorbas Basin shallow series has been computed. Validity of the model was ensured by extensive field survey constraining large-scale geometries but also to precise the relationships between the different sedimentary units. While 3D modeling is most of the time based on inversion of subsurface geophysical data, in this paper we present 3D modelling based on surface geological data which includes field structural measurements (orientations), observed contact points and geological map outlines. This new 3D modelling approach shows an internally consistent geometrical model as it reproduces the field-based geological map and observations from the scale of the whole basin to much larger scales. It is also used to analyze the geometry and morphology of the interpolated surface separating evaporitic and post-evaporitic series and thus decipher the relative impact of the MSC into the basin. From these new structural and geometrical constraints, we clarify the evolutionary scenario of the Sorbas basin from the Late Messinian to the Early Pliocene as follows: 1) Messinian gypsums are topped by an unconformity (the MES) that confirms the erosion of the basin; 2) the reflooding took place during the progressive shortening of the basin leading to the gravitational sliding of the Sorbas calcarenite and small-scale box-folding.

2. Geodynamic setting and stratigraphy

The Betic Cordillera forms the northern branch of the Betic-Rif orogenic belt resulting from the continental collision between the allochthonous Alboran domain and the Iberian margin (Platt *et al.*, 2003). The Internal Zones of the belt comprise a pile of overthrust metamorphic rock outcropping into E-W elongated metamorphic domes developed, later on, during orogenic extension (Martínez-Martínez and Azañón, 1997, 2002; Augier *et al.*, 2005a, 2005b). The Sorbas Basin is bounded by two of these domes: the Sierra de los Filabres to the North and the Sierra Alhamilla to the South (Fig. 1). It belongs to a mosaic of Late Neogene intramontane basins with the Tabernas, Vera and Níjar-Carboneras basins (Fig. 1; Ott d'Estevou and Montenat, 1990; Sanz de Galdeano and Vera, 1992; Pedrera *et al.*, 2010).

The sedimentary record of the Sorbas Basin starts with scarce Serravallian conglomerates (Ott d'Estevou and Montenat, 1990) covered by Tortonian shallow- to deep-marine sediments. Their deposition in the southern part of the Sorbas Basin was mostly controlled by the exhumation and emersion of the Sierra Alhamilla (Do Couto *et al.*, 2014). Messinian sediments overlap the Tortonian marine sediments with an angular unconformity and can be subdivided into six units (Fig. 2A). At the bottom of the series, the Azagador Member (U1, Fig. 2A) is composed of a shallow marine fossiliferous calcarenite that exhibits a conspicuous basal conglomerate (Ott d'Estevou and Montenat, 1990) dated from the Tortonian/Messinian boundary (Sierra *et al.*, 1993; Gautier *et al.*, 1994; Krijgsman *et al.*, 2001). The upper part of this unit passes laterally to an early Messinian upper bathyal and marly unit known as the Lower Abad Member (U2, Fig. 2A). Further up, the Upper Abad

Member (U3, Fig. 2A), is composed of marls alternating with diatomites suggesting more restricted but still open marine conditions. The uppermost part of the Abad Member passes laterally to fringing reefal carbonates outcropping both in the northern and in the southern part of the basin (e.g. Cariatiz and Morrón de la Cantona localities; Fig. 2A). Then, a rather thick evaporitic unit (Yesares Member) consisting in gypsum and clays alternation (U4, Fig. 2A) deposited during the MSC, from 5.971 to 5.6 Ma (Manzi *et al.*, 2013; Clauzon *et al.*, in revision). The Sorbas Member (U5, Fig. 2A) lies on top of the Messinian evaporites and is composed of a lagoonal calcarenite, laterally equivalent to clayey deltaic beds formed in more distal but shallow environment (Roep *et al.*, 1998). Last deposits of the Zorreras Member (U6, Fig. 2A) are mostly composed of reddish conglomeratic continental deposits interspersed with Pliocene fossiliferous marine sandstone (Montenat *et al.*, 1980; Fortuin *et al.*, 2000; Martín-Suárez *et al.*, 2000). The Sorbas (U5) and Zorreras (U6) members represent respectively the basinward extension of the subaqueous and subaerial parts of Gilbert-type fan deltas developed in the northern margin of the Sorbas Basin (Clauzon *et al.*, this volume).

The time gap separating the Yesares (U4) and Sorbas (U5) members, and the presence of the MES in the Sorbas Basin have been matters of an intense and still ongoing debate for several decades (Rouchy and Saint-Martin, 1992; Clauzon *et al.*, 1996; Roep *et al.*, 1998; Riding *et al.*, 1998, 2000; Martín *et al.*, 1999; Fortuin *et al.*, 2000; Krijgsman *et al.*, 2001; Braga *et al.*, 2006; Bourillot *et al.*, 2009; Roveri *et al.*, 2009; Clauzon *et al.*, in revision). While the contact between these two units is commonly regarded as conformable, in a continuous series, as suggested by some outcrops along the Río Aguas (center of the basin, see Fig. 2B; Dronkert, 1976; Ott d'Estevou and Montenat, 1990), this latter looks as unconformable in other parts of the basin (Clauzon *et al.*, in revision). These recent results show that the post-evaporitic unit most probably corresponds to the reflooding event postdating the drawdown of the Messinian Salinity Crisis. The time gap separating the evaporitic from post-evaporitic deposits is estimated from 50 (Roveri *et al.*, 2009) to 140 kyrs (Clauzon *et al.*, in revision; see the synthetic stratigraphic log in Fig. 2A); this corresponds to the massive drawdown of the Mediterranean Sea during the second step of the Messinian Salinity Crisis (Clauzon *et al.*, 1996; CIESM, 2008).

The terminology used in the literature and in this contribution to describe the time gap of sedimentation during the Messinian Salinity Crisis refers to this contact as the MES where the erosion is clearly visible (i.e. angular unconformity or development of subaerial alteration; zoom on Moras in Fig. 2C) or as the Messinian Discontinuity where erosional figures cannot be evidenced but where a similar time gap exists (see Melinte-Dobrinescu *et al.*, 2009).

3. Approach and theoretical background

This study aims to constrain the 3D geometry of the post-Tortonian series within the Sorbas Basin with a particular focus on the MES. 3D geometrical modeling is an important methodology used in geology to constrain and image local to regional-scale geological structures (e.g. Houlding, 1994; Mallet, 2002; Wu *et al.*, 2005), for a wide range of interpretations and calculations such as of sedimentary volumes or finite deformation quantities. In basin environments, 3D modeling approaches are typically based on boreholes data or seismic profiles interpretation. Given that no such underground data is available in the Sorbas area, a less classical approach is developed here where the shallow basin structure (+500 a.s.l. up to -50 m b.s.l.) is exclusively constrained by both new and existing field structural data and geological mapping. We used the 3D Geomodeller (BRGM – Intrepid Geophysics) software where geometries can be interpolated, in three dimensions, between data points. Details on the method are given in Lajaunie *et al.* (1997), Calcagno *et al.* (2008) or Guillen *et al.* (2008). Here, the 3D geometrical interpolation is based on both the location of geological interfaces where they are observed (including faults or stratigraphic contacts) and structures orientation measured within the units (fault planes and bedding orientations). The 3D interpolation is performed through a co-kriging (Calcagno *et al.*, 2008). During the modeling process, the sequence of interpolation of the geological units is given by a synthetic geologic pile which takes into account the nature of the contacts separating units:

“erosive” in case of an unconformity or cross-cutting type or “onlap” in case of a sedimentary filling. This step is crucial to ensure the geometrical relationships observed from the field to the computed model. The thickness of the sedimentary formations is neither input nor fixed in the modeling process because each formation will be modelled from its lower and upper bounding surfaces. Such computation allows varying the relative thickness of each formation according to the nature of its bounding surfaces.

From the data acquired and a compilation of existing data (Fig. 3), a 3D model is built at the scale of the overall basin through a geometrical interpolation between the measured orientation data and the geological contacts. Based on a “trial and error” process, the 3D geometry is further adjusted by adding isolated and scarce control points in order to fit the 2D geological map view produced by the model with the geological map of the basin drawn in the field independently. Indeed, outlines pattern of geological boundaries on a map depend on the local obliquity between the geological surfaces (bedding, boundaries, faults, etc.) and the surface topography. As the relief is rather hilly throughout the study area and as sedimentary layers most often have moderate dip throughout the basin, geological boundaries display various outline patterns in the geological map with rather contorted shapes in some places (Fig. 1). It is worth noting that a 10 m high resolution Digital Elevation Model (DEM) was used for computations in order to avoid scale problems. For the entire area considered (dashed rectangle in Figure 1), more than 500 field observations have been compiled and used for modeling. The 3D model interpolation is considered to be valid when the 2D geological map view extracted from the model fits the field-based geological map of the area. As a whole, this procedure yields an internally consistent geometrical model of the Sorbas Basin with the geological structures drawn in the map and cross-sections entirely compatible in 3D. Surfaces and geological bodies can be extracted from the 3D model to analyze their morphology and geometry. We used this extraction to analyze the morphology of the Messinian unconformity.

Another 3D model was computed at larger scale for the southwestern part of the Sorbas Basin, south of Sorbas City (see location in Figure 3), in order to consider and study some peculiar folds observed in the sediments of that part of the basin (see details below). Here, interpolating parameters were adjusted to better fit the bedding orientation measured and to reproduce local variations in the sedimentary layers structure.

4. Field constraints

4.1. Basin-scale structure

The current structure of the Sorbas Basin displays a roughly E-W trending syncline geometry (Fig. 2B, 2C). At Morrón de la Cantona area (to the south), calcarenites of the Azagador Member lie unconformably over the steeply dipping Tortonian series. In turn, post Tortonian deposits are locally gently folded (see Fig. 2, to the south). From the Azagador Member up to the Yesares Member gypsum deposits, the sedimentary layers all look conformable as measured bedding orientations are often sub parallel (Fig. 2C). While the Azagador Member displays a homogenous lithology and outlines a rather simple structure, the structure of deposits from the gypsum upward is more complicated with (i) rapid lateral transitions in the sedimentary facies, (ii) the imprint of the Messinian Erosional Surface as well as (iii) small wavelength folding of the gypsum and overlying series to the south (Fig. 2C). From Tortonian and up to, at least, the Sorbas Member, the series of the Sorbas Basin displays a progressive decrease in fold amplitude; such feature most certainly results from an ongoing N-S compression active since the late Tortonian (Galindo-Zaldívar *et al.*, 1993; Augier *et al.*, 2013; Do Couto *et al.*, 2014).

A new geological map was drawn based on field observations (Fig. 3), interpretation of aerial ortho-photographs and a precise digital elevation model together with available maps (García Monzón *et al.*, 1972, 1973a, 1973b, 1974; Ott d'Estevou and Montecat, 1990). More than 500 observation sites have been analyzed in the basin (red dots in Figure 3) with more than 300 structural measurements in particular in the central part of the basin, among which the most important are shown in Figure 3.

4.2. Structure of the post MSC deposits

A detailed cross-section realized from the Zorreras hill to the Barranco del Infierno area (Fig. 4A), shows progressive facies lateral transitions between clay-rich bottomset beds and coastal coarse-grained deposits (U5; Fig. 2A) over the Messinian gypsum (U4; Fig. 2A). The calcarenite and sandstone layers composing the Sorbas Member are distributed over the western to southwestern part of the Sorbas Basin, and more particularly on its southwestern uplifted flank (Fig. 2B,C). The compressional deformation affected the basin during the Pliocene as the surface separating the submarine sediments from the subaerial ones (i.e. the marine-continental transition between U5 and U6; Fig. 2A) is presently folded. As displayed along N340 road, in the surroundings of Sorbas City, the reddish continental conglomerate of the topset beds of the deltaic system (U6; Fig. 2A) thins southward (passing from more than 50 m to less than 10 m thick; Fig. 4B).

The base of the Zanclean sequence, including the Sorbas calcarenite and its lateral equivalent in the clayey to marly facies (U5), truncates the underlying Yesares Member gypsum layers (Clauzon *et al.*, in revision). In order to refine the geometry and origin of that particular surface, we focused on the base of the post-evaporitic deposits around the basin, from the proximal output of a Gilbert-type fan delta to the north (Góchar and Moras localities, Fig. 2A), to its more distal parts to the south. In the Barranco del Infierno area, the overview of the Messinian discontinuity (Fig. 5) displays the geometric relationship between the northward dipping Yesares Member gypsum and the horizontal Sorbas Member (Fig. 5A, B). As the gently bended gypsum layers lie horizontally in the center part of the basin, the contact in-between these two units appears geometrically conformable at the base of the gully (dashed red line in Fig. 5B). However, detailed observations of that interface along the ravine show that the Messinian gypsum (U4) is separated from the overlying Sorbas Member (U5) by an erosional surface (Fig. 5C) which probably corresponds to the MES. A yellowish to reddish conglomerate, containing small and well-rounded pebbles locally occurs below the Sorbas Member along the MES (Fig. 5D). Such a feature may attest for subaerial erosion which is consistent with the peak of the MSC (Clauzon *et al.*, in revision).

4.3. Small scale folding

In the Barranco del Infierno area, the Sorbas Member appears folded above the Yesares Member gypsum (Fig. 6). Cross-section 1 (Fig. 6A) illustrates the geometry of the shallow marine calcarenite belonging to the Sorbas Member (U5): the Messinian gypsums (U4) visible in the background, to the southeast, display a homogeneous north-dipping geometry. Conversely, the shallow marine calcarenite exhibits small-scale 3D folding with a N25-30°E striking principal axis direction and a N90-100°E second order one (Fig. 6A). It is to be noted that part of the Messinian gypsum series (U4) crops out in the core of one of the anticlines to the southwest of the creek (Fig. 6A).

Cross-section 2 (Fig. 6B) illustrates diverging dips around a dome-like antiform termination of such small-scale folding where bedding orientations vary from 18-20°W to ~50°S-SW. While most of the folds are open (Fig. 6A, B), some of the synclines can be quite tight (Fig. 6A, 7A), and the upper Zorreras Member filling the depressions displays syn-tectonic growth-strata structures (Cross-section 3; Fig. 7B), highlighting syn-sedimentation folding. These structures are of much shorter wavelength than the general folding of the series, as presented above. They affect a rather large area to the south but are restricted to the southern limb of the Sorbas Basin.

5. 3D modeling and interpretation

Series of the Sorbas Basin display a regional E-W oriented open syncline and more local small-scale folds superimposed to the south; this implied to develop two distinct modeling approaches with different resolutions to properly render the structure geometry. Indeed, from a very general point of view, the variance level into a data set may depend upon the width of the sampled area considered and thus interpolation processes leads to different degrees of smoothing when changing scale. In our case study, and as detailed

below, different statistical parameters must be defined when modeling 3D geometries of the overall basin infilling or of the shorter wavelength folding to the south.

5.1. Overall geometry of the basin

Following the above detailed methodology, a first 3D model was computed for the shallow structure of the Sorbas Basin based on i) field structural observations and measurements, ii) digital elevation model and iii) mapped outlines of the geological boundaries which highly depend on the local orientation of the geological surfaces (cf. geometrical intersection of bedding, boundaries or faults with topography). At first, based on the stratigraphic log of the basin (Fig. 2A) and the nature of the contact separating geological units (e.g. conformity/unconformity), a synthetic geologic pile was conceived. This pile takes into account angular unconformities as observed at the base of the Azagador Member and on top of the Yesares Member. Besides, based on field observations, marls of the Abad Member and the overlying Messinian reefal limestones (U3; Fig. 2A) belong to the same stratigraphic unit and were grouped into a single ensemble for modeling (i.e. with concordant and laterally continuous bedding; Fig. 2, 8A). In the same way, the bottomset beds of the Gilbert-type fan delta and the calcarenites of the Sorbas Member (representing its distal subaqueous lateral equivalent) are also considered as a unique sedimentary unit for computation (U5; Fig. 2, 8A).

The modeled area covers 290 km² (see dashed rectangle in Figure 1) and extends 5 km at depth. For the overall 3D volume considered, 476 bedding orientation measurements (out of a total of 503 observation sites, see red dots in Figure 3) were used to constrain the attitude of the geological interfaces into the basin together with 273 contact points scattered across the map and along three cross sections for a few of them (see Supplementary data). Note that computation of the 3D geometrical model of the post-Tortonian deposits of the Sorbas Basin does not only depend on the known location for the geological interfaces but more strongly on the structural measurements which can be done both along the geological boundaries and into the geological formations themselves. Then, the geometry of the 3D model is adjusted so as to reproduce the geological boundaries from the map (Fig. 2). At first order, many similarities can be observed between the field-based geological map and the map view of the model. It includes the main unconformities (black arrows in Fig. 8B, C), sedimentary “windows” and *cuestas* (see Rambla de Góchar and Moras, Cerro Colorado and El Cerrón localities in Fig. 8B, C) which highly depend on the sedimentary layers strike and dip values. The spatial distribution of outcropping geological layers, as for instance that of the Pliocene Gilbert-type fan deltas (U5 and U6) with respect to the Yesares Messinian gypsums (U4), is also well modeled. As shown in figures 1 and 8B, a large part of the Sorbas Basin area, to the North, exposes reddish conglomeratic deposits of the Zorreras Member forming a gently south-dipping back slope (see Fig. 2). These layers stand for the topset beds of Gilbert-type fan deltas that cover and hide most of the earlier structure of the deposits in that area. However, the underlying series are pretty well exposed along river incisions and the locations of the modeled geological boundaries along these incisions well coincide with those observed in the field, in particular along the Río Aguas, Moras and Góchar valleys (compare Fig. 8B and 8C). In details, some local discrepancies however remain on the modeled geological map, as it is the case to the east of the model where the Tortonian-Messinian calcarenite of the Azagador Member (in brown) displays a lesser outcropping extent than observed in the field (Fig. 8). This misfit may be due to the lack of field constraints in that area and/or to the peculiar structural relationship of this formation with surrounding layers, as observed in the nearby Morrón de la Cantona area. To better highlight the reliability of the modeled geological map, a close-up view has been performed in the central part of the basin (Fig. 8D, E) where stratification lies sub-horizontally (Fig. 5A, B) and meanders of the Río Aguas and its tributaries create a rather complex pattern of valleys (Fig. 5B, 8D). Given such a structural configuration, small changes in bedding or boundaries strike/dip must induce large modifications of the shape and position of the outline of geological boundaries on the map. Despite this complexity, the geological map computed from the 3D model sustains all the major geological features observed in that part of the basin (and drawn in the geological

map): the tabular distribution of the Zorreras Member (compare Fig. 8D, 8E) surrounding the Sorbas City and draping the highlands as back slope; similar local erosion features located along the Río Aguas River and its tributaries (Barranco del Infierno and Barranco del Hueli); and the North verging V-shaped morphology of the gypsum series in Cortijo del Hoyo area, marking the MES orientation. There, the marine clays of the Sorbas Member (U5) are separated from the Yesares Messinian gypsum (U4) by the Messinian Erosion Surface (Fig. 9A, B; Clauzon *et al.*, in revision). Results of the 3D modeling fairly represent the erosion between these two sedimentary units, predicting a low dipping unconformity extending over 3 kilometres (Fig. 9C).

5.2. Messinian Erosional Surface and gypsum spatial distribution patterns

The Messinian unconformity (e.g. separating deposits preceding the peak of the Messinian Salinity Crisis - the second, huge, sea-level drop - from those following it) is extracted as an elevation surface from the computed 3D model and analyzed to unravel its unconformable character. The computed 3D model allows appraising the geometry of this surface in its entirety, i.e. for the entire basin scale. The contour map of that surface shows a flat and rather high minimum altitude North and East of Sorbas City (Fig. 10A). Two N-S oriented corridors from the Góchar-Moras and Cariatiz areas reach the lower level (Fig. 10A, B); there, contours display curved and tight shapes and a relatively steep geometry of the surface. As these corridors have been filled up by the submarine part of Gilbert-type fan deltas later on, these can easily be interpreted as south-directed palaeo-valleys (see green arrows on Fig. 10A) and this erosional surface can be ascribed to the Messinian Erosional Surface (i.e. angular unconformity). Interpretations from the 3D model confirm local field observations of this surface made at different locations of the basin (see Barranco del Infierno, Fig. 6; Cortijo del Hoyo, Fig. 8D, 9) showing an erosional contact between the pre- and post-MSC deposits (Clauzon *et al.*, in revision). On the other hand, in the center of the basin, the tabular geometry of the Messinian gypsum layers and overlying Pliocene bottomset beds has usually been ascribed to a continuous stratigraphic transition (Fortuin *et al.*, 2000; Krijgsman *et al.*, 2001; Bourillot *et al.*, 2010). The 3D modeling of the Messinian unconformity confirms the relatively flat geometry of that surface (see North and East of Sorbas City; Fig. 10A). However, its continuity across the basin combined with the recently estimated time gap separating Messinian from Pliocene deposits (Clauzon *et al.*, in revision) show that this latter can be interpreted as the Messinian Discontinuity. The modeled 3D geometry of the sedimentary series highlights that geometrical relationships between units, and in particular along the MES, drastically change across the basin because of the large scale ~E-W trending fold imaged. Indeed, the different layers of the basin display contrasted amplitudes in the fold suggesting continuous folding during sedimentation. This leads to different angular relationships between layers from the hinge to the limbs of the basin-scale fold.

For modeling purpose, the geometry of the Messinian unconformity has been constrained by ~20 geolocalized checkpoints where the surface has been directly observed in the field (and more particularly in the Barranco del Infierno area). Its geometry has also been constrained by ~25 checkpoints within the underlying Messinian gypsum layers and ~130 within the above lying coastal deposits which provide, respectively, the lowermost and uppermost possible locations for the modeled interface in the 3D block considered. Figure 10B displays the current thickness of the gypsum deposits (below the late Messinian-Zanclean Gilbert-type fan delta deposits) as modeled in this study. The largest thickness, around 120 m, is located in the northeastern part of the studied area, where exposed gypsum layers are extracted from two quarries near Cariatiz (Cruz de Rojo and Peñon Diaz, Fig. 10B). This thick gypsum accumulation, alternating with fossiliferous marine marly to clayey layers, near the top of the series (Montenat *et al.*, 1980; Saint-Martin *et al.*, 2000; Goubert *et al.*, 2001; Clauzon *et al.*, in revision) extends from south of Cariatiz to Cerrón de Hueli (Fig. 1) where it forms the highest culmination point of the outcropping gypsum Formation. The western gypsum accumulation (Fig. 10B) corresponds to the gypsum deposition observed and described by Ott d'Estevou and Montenat (1990). It is to be noted

that such location of gypsum remains speculative at this stage. The thickness map of the gypsum Yesares Member obviously shows lateral irregular distribution with two remarkable features: (i) a large area where gypsum is missing, below the Góchar and Moras Gilbert-type fan deltas, in the north-central part of the basin and (ii) two narrow parts, with limited thicknesses, in the southwestern part of the basin (see black ellipses in Fig. 10B).

5.3. High resolution 3D modeling of short wavelength folds

In the Barranco del Infierno area, the Sorbas Member (U5) displays rather short wavelength folding as observed in the field. Due to scale effect, 3D modeling of the overall shallow basin geometry, as detailed above, cannot account for the geometry of such small scale structures. Indeed, modeling is performed through a joint kriging interpolation between locations of interface data points and structural orientations (see above) and for such computation, very local variations in the data may be integrated in the nugget effect parameter which is regarded as noise relative to the regional-scale variations. As far as this kind of strata folding is restricted to the particular case of the Barranco del Infierno area, such fold wavelength cannot be modeled with the above described basin scale 3D structural model.

Another more precise 3D model was thus computed for the restricted area of the Barranco del Infierno (Fig. 11). Structural data set was densified there; 107 bedding orientations were measured throughout the Sorbas Member across a ~800 m by ~600 m wide area (Fig. 11A). Calcarenite often displays gentle to moderate dips and a few horizontal planes were measured in particular on top of the hills forming the local topography (Fig. 11A). Stereographic projection of poles to bedding measurements clearly shows scattering of the orientations, both in strike and dip, with a roughly horizontal average dip value (Fig. 11B). New interpolation parameters were also used compared to the large scale model: (i) in the field, structural analysis of the area shows shorter wavelength folds (Fig. 6) and a distance of 250 m was thus used as the range value for kriging interpolation (i.e. maximum correlation distance), (ii) the nugget effect was reduced close to zero in order to avoid over-smoothing of the orientation data by local variations during 3D model computation. Two distinct series were defined for this local 3D model: one for the Yesares Messinian gypsum at the base (in purple on Figs. 12, 13 and 14) and one for the Sorbas Member. In order to easily illustrate the attitude of the interpolated bedding, the Sorbas Member was discretized in ten layers (see dark to light green for younging layers on Figs. 12, 13 and 14). The resulting 3D model well reproduces two gypsum “windows” outcropping in valleys of the central and northeastern parts of the area (Fig. 12A). The interpolated geometries also fit well the structures observed in the field such as an anticline pretty well exposed along the right bank of the Barranco del Infierno (compare Fig. 6A and Fig. 12B, in the central part of the model). The base of the Sorbas Member (i.e. the top of the gypsum) displays rather contorted geometries with domes and saddles shaped structures (Fig. 12C). Undulation varies from 335 to a maximum absolute height of 435 m (Fig. 12D) with fold amplitude of ~75 m on average.

Though contours generally look isotropic, two principal orientations may be deciphered: one trending N25 to N30°E and the other one trending N90 to N100°E (Fig. 12D). Horizontal slices through the model allow comparing the trace of the interpolated bedding at a given altitude (which could be compared to trajectories map applied to bedding striking) to the bedding orientation measured at about the same height (Fig. 13). Due to the very limited nugget effect value used for modeling here, interpolated interfaces trend almost parallel to the original measurements from 400 to 450 m high (Fig. 13), showing a robust consistency between the measurements and the model.

Structural interpretation of these projection maps clearly highlights the same two preferential folding directions in the area (N25-30°E and N90-100°E). Though fold amplitude laterally varies in the area (as shown by changes in structural levels illustrated in the maps), the fold envelope displays a simple northward tilting. Finally, independently of their strike, cross sections display similar fold shapes with rather tight synclines compared to the open anticlines (Fig. 14). Measured wavelength of the folds ranges from 250 to ~350 m in the model (Fig. 13). As shown in the model, development of the “nearly” box-fold type

geometries of the anticlines together with their very pronounced non-cylindrical attitude may be linked to the presence of the underlying gypsum in the Barranco del Infierno area. Such lithology may have acted as a decollement layer during deformation of the overlying series.

6. Discussion

6.1. Structure of the post-Tortonian series

Based on an inversion of geological and structural field observations and measurements, the 3D modeling allows precisely determining the large-scale finite geometry of the shallow Sorbas Basin deposits. As a whole, the Sorbas Basin displays a rather large wavelength east-trending syncline in consequence of a ~N-S shortening. However, the highly deformed late Tortonian series contrasts with the open fold geometry of post-Tortonian deposits (Do couto et al., 2014). Everywhere, except to the south-southwest of the basin, the shallow deposits of the basin highlight smooth structures and geometrically continuous layers with only few and limited faults. In contrast, the southern flank of this large syncline shows second order folding with shorter wavelength and a complex 3D geometry. There, coastal facies of the Sorbas Member, laterally passing to basin clays equivalent to bottomset beds, was deposited on the southwestern highest flank of the basin. Field structural analysis combined with large-scale 3D modeling show that the Sorbas Member calcarenite displays dome-shaped folds with very oblique axes (N25-30°E and N90-100°E) and small-amplitude (250 to 350m). Moreover, while anticlines are clearly open, synclines are sometimes very tight. All these features are compatible with folding developed above a decollement layer, with a high competency contrast. At this stage, the relative contribution of tectonic deformation *versus* gravity-driven folding cannot be appreciated, but, given that those structures developed along the rather steep southern flank of the syncline basin, it seems conceivable that part of the deformation was caused by northward gravitational sliding over the Yesares Messinian deposits during tilting of the underlying series. Its latter deformation over the Yesares Messinian gypsum was accompanied by the syn-tectonic deposition of the subaerial Zorreras Member. Although two oblique fold axes, none of them appears to refold the other one and are therefore considered to occur simultaneously, thanks to a single constrictional deformation event.

Given the dome shaped geometry of the folds and their core composed of gypsum, one may think that the deformation is the result of diapirism. Diapirism may be driven by different mechanisms such as buoyancy forces, basal slope, tectonic stresses, erosion of the overburden layers or even differential loading (Hudec and Jackson, 2007; Brun and Fort, 2011). In the studied area, the fact that the gypsum series only crops out in the core of few folds does not allow to study its internal structure in detail. At first sight, gypsum appears relatively undeformed and unweathered and may represent the early stage of diapirism.

Accordingly, the deformation observed in the southern flank of the Sorbas Basin may have induced by (i) tectonic shortening, (ii) gravity sliding of the area along the southern flank or (iii) early stages of diapirism.

6.2. Fluvial drainage

The inland Sorbas Basin offers very good exposure conditions to study the history of the Messinian Salinity Crisis and its effects on sedimentation and structures. During the late Messinian, restriction of the Sorbas Basin resulted in the deposition of an evaporitic formation, in the central part of the basin, which locally reached a thickness of, at least, 120 m. During the paroxysm of the Messinian Salinity Crisis, the major sea-level drop left the Sorbas Basin under the effect of subaerial erosion that shaped the landscape in widespread karsts and deeply cutting Messinian fluvial valleys. When the marine reflooding of the Mediterranean Basin reached the Sorbas Basin in the latest Messinian, Gilbert-type fan deltas filled the tectonically enhanced accommodation space together with Messinian valleys. The Sorbas Basin was momentarily reconnected to the sea. Gypsum isobaths computed from the 3D model of this study (Fig. 10) provide useful information about the possible exit of the Messinian valleys from the basin realm at that time. The topmost residual architecture of the gypsum series displays an irregular morphology as the most significant

erosion is located downstream Góchar and Moras Messinian valleys (Fig. 10), nowadays filled by Early Pliocene deltaic sediments belonging to the Sorbas Member (Clauzon *et al.*, in revision). From West to East, this palaeogeographic depression is surrounded by thick gypsums that do not exhibit deep erosional features compared to its central part (Fig. 10). At least two main reasons can explain this apparent hiatus (i) the initial lack of evaporites (i.e. non-deposition hiatus) or (ii) the erosion of evaporites due to the subaerial exposure of the basin during the peak of the MSC (i.e. erosional hiatus). Considering the syncline geometry of the basin and the lack of any structure preventing deposition of gypsum in the center of the basin, the erosion of gypsum layers is the most probable hypothesis. These results support the development of an overall South to Southeast-verging erosive system that was active during the peak of the MSC. The N-S oriented fluvial network, probably connected to a watershed originating in the Sierra de Los Filabres, may have used a southern outlet to exit the Sorbas Basin. The recent (Early to Mid-Pleistocene) rerouting of the Río Aguas River eastward (Harvey and Wells, 1987; Stokes *et al.*, 2002) probably erased a large part of this ancient drainage system.

Based on the existence of Pliocene marine deposits in the Vera and Níjar-Carboneras basins, two possible seaways are supposed to co-exist between the Sorbas and Vera basins through the Alfaix corridor (Fig. 1; Braga *et al.*, 2003; Stokes, 2008) and between the Sorbas and Níjar-Carboneras Basin through the Polopos sill (Fig. 1; Martín *et al.*, 1999; Fortuin and Krijgsman, 2003). The existence of a seaway through the Polopos sill is also considered because of the occurrence of South-dipping fluvio-deltaic systems in the northwestern part of Níjar-Carboneras Basin during the Lower Pliocene (Aguirre, 1998; Aguirre and Sánchez-Almazo, 2004). These fluvio-deltaic deposits known as the Feos Formation unconformably overly the Messinian gypsum and limestone above an erosional surface considered as the Messinian Erosional Surface (Omodeo-Salé *et al.*, 2012). Such valley incision suggests that a fluvial network shaped the landscape during the peak of the MSC. Its origin and its watershed extension are unknown and the absence of Lower Pliocene deposits between the two basins stands in the way of this suspected connection. However, based on our observations and the recent capture of the Río Aguas River eastward (Harvey and Wells, 1987; Stokes *et al.*, 2002), we assume that the Sorbas Messinian valley made its way towards the Níjar Basin.

7. Conclusive remarks

The imprints of the Messinian Salinity Crisis in the Sorbas Basin have been a matter of debate for a long time. Our 3D modelling based on surficial data (bedding orientations, intersections with topography) and field observations shows the predicted geometry of the Messinian Erosional Surface at depth. The overall geometry of the MES confirms its erosive character at the base of the post-MSC deposits consisting of deltaic deposits. Its morphology reveals the occurrence of two main N-S oriented valleys dipping toward the center of the basin. These valleys are currently filled by post-MSC deltaic deposits which fossilized the MES. Such an incision suggests that a fluvial network shaped the landscape during the peak of the MSC. However, its origin and its watershed extension are still unknown. We infer that a fluvial connection persisted between the Sorbas and Níjar Basin during the peak of the MSC and a marine one after the Mediterranean reflooding.

More locally, we show that deformations can superimpose the irregular shape of the MES. Indeed, in the Barranco del Infierno area, small-scale folding describes box-type folds oriented along two oblique NNE-SSW and NW-SE fold axes. The peculiar geometry of these folds may have been formed (1) through the gravitational sliding of the Sorbas shallow calcarenite over the Messinian evaporites during the progressive tilting of the southern flank of the basin or (2) during the early stages of diapirism. Growth-strata structures observed in the overlying reddish continental conglomerates belonging to the Zorreras Member ensure a confident Zanclean age constraint for the deformation.

From a methodological point of view, the original approach developed consists in modeling the shallow structure of a sedimentary basin based on field observations and geological mapping. Application of this approach in the case-study of the Sorbas Basin

shows that the use of 3D modeling – such as with the 3DGeomodeller – can highly help imaging geometry and structures of a sedimentary basin.

8. Acknowledgments

This work was suggested by the late Georges Clauzon. Field investigations have been supported by the CIFRE PhD grant N° 584/2010 (TOTAL/UPMC). 3D modeling process was performed using the 3D Geomodeller (Intrepid Geophysics) developed by the BRGM (Orléans, France). We are grateful to Gabriel Courrioux (BRGM-GEO) for providing us a 3D Geomodeller licensing and for his technical support. We wish to thank Alexandre Lethiers for his support for the illustrations. We acknowledge Ana Crespo-Blanc and an anonymous reviewer for their constructive remarks.

References

- Aguirre, J., 1998. El Plioceno del SE de la Península Ibérica (provincia de Almería). Síntesis estratigráfica, sedimentaria, bioestratigráfica y paleogeográfica. *Rev. Soc. Geol. España* 11, 297-315.
- Aguirre, J., Sánchez-Almazo, I.M., 2004. The Messinian post-evaporitic deposits of the Gafares area (Almeria-Nijar basin, SE Spain). A new view of the “Lago-Mare” facie. *Sedimentary Geology* 168, 71-95.
- Augier, R., Agard, P., Monié, P., Jolivet, L., Robin, C., Booth-Rea, G., 2005a. Exhumation, doming and slab retreat in the Betic Cordillera (SE Spain): in situ $^{40}\text{Ar}/^{39}\text{Ar}$ ages and P–T–d–t paths for the Nevado-Filabride complex. *J. metamorphic Geol.* 23, 357-381.
- Augier, R., Booth-Rea, G., Agard, P., Martínez-Martínez, J.M., Jolivet, L., Azañón, J.M., 2005b. Exhumation constraints for the lower Nevado-Filabride Complex (Betic Cordillera, SE Spain): a Raman thermometry and Tweeku multiequilibrium thermobarometry approach. *Bull. Soc. Géol. Fr.* 176, 403-416.
- Augier, R., Jolivet, L., Do Couto, D., Negro, F., 2013. From ductile to brittle, late- to post-orogenic evolution of the Betic Cordillera: Structural insights from the northeastern Internal zones. *Bull. Soc. Géol. Fr.* 184, 405-425.
- Bourillot, R., Vennin, E., Rouchy, J.M., Durlet, C., Rommevaux, V., Kolodka, C., Knap, F., 2009. Structure and evolution of a Messinian mixed carbonatesiliciclastic platform: the role of evaporites (Sorbas Basin, South-east Spain). *Sedimentology* 57, 477-512.
- Bourillot, R., Vennin, E., Rouchy, J.M., Blanc-Valleron, M.M., Caruso, A., Durlet, C., 2010. The end of the Messinian Salinity Crisis in the western Mediterranean: Insights from the carbonate platforms of south-eastern Spain. *Sedimentary Geology* 229, 224-253.
- Braga, J.C., Martín, J.M., Quesada, C., 2003. Patterns and average rates of late Neogene–Recent uplift of the Betic Cordillera, SE Spain. *Geomorphology* 50, 3-26.
- Braga, J.C., Bassi, D., Martín, J.M., Riding, R., Aguirre, J., Sánchez-Almazo, I.M., Dinarès-Turell, J., 2006. Testing models for the Messinian salinity crisis: The Messinian record in Almería, SE Spain. *Sedimentary Geology* 188-189, 131-154.
- Brun, J.-P., Fort, X., 2011. Salt tectonics at passive margins: Geology versus models. *Marine and Petroleum Geology* 28, 1123-1145.
- Calcagno, P., Chilès, P., J., Courrioux, G., Guillen, A., 2008. Geological modelling from field data and geological knowledge: Part I. Modelling method coupling 3D potential-field interpolation and geological rules. *Phys. Earth Planet. Inter.* 171, 147-157.
- CIESM, 2008. The Messinian Salinity Crisis from mega-deposits to microbiology - A consensus report, in: Briand, F. (Eds.), CIESM Workshop Monographs. CIESM, 16 bd de Suisse, MC-98000, Monaco, p. 168.
- Clauzon, G., Suc, J.-P., Gautier, F., Berger, A., Loutre, M.F., 1996. Alternate interpretation of the Messinian salinity crisis: Controversy resolved? *Geology* 24, 363-366.
- Clauzon, G., Suc, J.-P., Do Couto, D., Jouannic, G., Melinte-Dobrinescu, M.C., Jolivet, L., Lebreton, N., Mocochain, L., Popescu, S.-M., Martinell, J., Doménech, R., Rubino, J.-L., Gumiaux, C., Warny, S., Gorini, C., Bache, F., Rabineau, M., and Estrada, F. New insights on the Sorbas Basin (SE Spain): the onshore reference of the Messinian Salinity Crisis. *Basin Research*, in revision.

- Conesa, G., Badinot, J.F., 1999. Early Messinian carbonate platforms from Sorbas Basin (S.E. Spain): sedimentary setting, microfaunas and palaeoenvironments. *Revue de micropaléontologie* 42, 255-267.
- Dabrio, C.J., Polo, M.D., 1995. Oscilaciones eustáticas de alta frecuencia en el Neógeno superior de Sorbas (Almería, sureste de España). *Geogaceta* 18, 75-78.
- Do Couto, D., Gumiaux, C., Augier, R., Lebret, N., Folcher, N., Jouannic, G., Jolivet, L., Suc, J.-P., Gorini, C., 2014. Tectonic inversion of an asymmetric graben: insights from a combined field and gravity survey in the Sorbas basin. *Tectonics*, 2013TC003458.
- Dronkert, H., 1976. Late miocene evaporites in the Sorbas Basin and adjoining areas. *Mem. Soc. Geol. It.* 16, 341-361.
- Fortuin, A.R., Krijgsman, W., Hilgen, F.J., Sierro, F.J., 2000. Late Miocene Mediterranean desiccation: topography and significance of the 'Salinity Crisis' erosion surface on-land in southeast Spain: Comment. *Sedimentary Geology* 133, 167-174.
- Fortuin, A.R., Krijgsman, W., 2003. The Messinian of the Nijar Basin (SE Spain): sedimentation, depositional environments and paleogeographic evolution. *Sedimentary Geology* 160, 213-242.
- Galindo-Zaldívar, J., González-Lodeiro, F., Jabaloy, A., 1993. Stress and palaeostress in the Betic-Rif cordilleras (Miocene to the present). *Tectonophysics* 227, 105-126.
- García Monzón, G., and Kampschuur, W., 1972. Mapa geológico de España, Hoja 1014, Vera, Instituto Geológico y Minero de España (IGME), Ministerio de Industria y Energía, Madrid, scale 1:50000.
- García Monzón, G., G., Kampschuur, W., and Vissers, R.L.M., 1973a. Mapa geológico de España, Hoja 1013, Macael, Instituto Geológico y Minero de España (IGME), Ministerio de Industria y Energía, Madrid, scale 1:50000.
- García Monzón, G., G., Kampschuur, W., Vissers, M., R.L., Verburg, J., and Wolff, R., 1973b. Mapa geológico de España, Hoja 1030, Tabernas, Instituto Geológico y Minero de España (IGME), Ministerio de Industria y Energía, Madrid, scale 1:50000.
- García Monzón, G., G., Kampschuur, W., and Verburg, J., 1974. Mapa geológico de España, Hoja 1031, Sorbas, Instituto Geológico y Minero de España (IGME), Ministerio de Industria y Energía, Madrid, scale 1:50000.
- Gautier, F., Clauzon, G., Suc, J.-P., Cravatte, J., Violanti, D., 1994. Age et durée de la crise de salinité messinienne. *C.R. Acad. Sci. Paris* 318, 1103-1109.
- Goubert, E., Néraudeau, D., Rouchy, J.M., Lacour, D., 2001. Foraminiferal record of environmental changes: Messinian of the Los Yesos area (Sorbas Basin, SE Spain). *Palaeogeography, Palaeoclimatology, Palaeoecology* 175, 61-78.
- Guillen, A., Calcagno, P., Courrioux, G., Joly, A., Ledru, P., 2008. Geological modelling from field data and geological knowledge: Part II. Modelling validation using gravity and magnetic data inversion. *Phys. Earth Planet. Inter.* 171, 158-169.
- Harvey, A.M., Wells, S.G., 1987. Response of Quaternary fluvial systems to differential epeirogenic uplift: Aguas and Feos river systems, southeast Spain. *Geology* 15, 689-693.
- Houlding, S.W., 1994. 3D Geoscience Modeling, Computer Techniques for Geological Characterization. Berlin, Springer Verlag, Germany, 309 pp.
- Hudec, M.R., Jackson, M.P.A., 2007. Terra infirma: Understanding salt tectonics. *Earth-Science Reviews* 82, 1-28.
- Hsü, K., Ryan, W.B.F., Cita, M.B., 1973. Late Miocene Dessication of the Mediterranean. *Nature* 242, 240-244.
- Krijgsman, W., Fortuin, A.R., Hilgen, F.J., Sierro, F.J., 2001. Astrochronology for the Messinian Sorbas basin (SE Spain) and orbital (precessional) forcing for evaporite cyclicity. *Sedimentary Geology* 140, 43-60.
- Lajaunie, C., Courrioux, G., Manuel, L., 1997. Foliation fields and 3D cartography in geology: Principles of a method based on potential interpolation. *Mathematical Geology* 29, 571-584.
- Mallet, J.L., 2002. *Geomodeling*: New York, Oxford University Press, 624 pp.

- Manzi, V., Gennari, R., Hilgen, F., Krijgsman, W., Lugli, S., Roveri, M., Sierro, F.J., 2013. Age refinement of the Messinian salinity crisis onset in the Mediterranean. *Terra Nova* 25, 315-322.
- Martín, J.M., Braga, J.C., Sánchez-Almazo, I.M., 1999. The Messinian record of the outcropping marginal Alboran basin deposits: significance and implications, in: Zahn, R., Comas, M.C., Klaus, a., (Eds.), A. (Eds.), *Proceedings of the Ocean Drilling Program, Scientific Results*, pp. 543-551.
- Martínez-Martínez, J.M., Azañón, J.M., 1997. Mode of extensional tectonics in the southeastern Betics (SE Spain): Implications for the tectonic evolution of the peri-Alboran orogenic system. *Tectonics* 16, 205-225.
- Martínez-Martínez, J.M., Soto, J.I., Balanyá, J.C., 2002. Orthogonal folding of extensional detachments: Structure and origin of the Sierra Nevada elongated dome (Betics, SE Spain). *Tectonics* 21, TC001283.
- Martín-Suárez, E., Freudenthal, M., Krijgsman, W., Fortuin, R., A., 2000. On the age of the continental deposits of the Zorreras member (Sorbas Basin, SE Spain). *Geobios* 33, 505-512.
- Melinte-Dobrinescu, M.C., Suc, J.P., Clauzon, G., Popescu, S.M., Armijo, R., Meyer, B., Biltekin, D., Cagatay, N., M., Uçarkus, G., Jouannic, G., Fauquette, S., Cakir, Z., 2009. The Messinian Salinity Crisis in the Dardanelles region: Chronostratigraphic constraints. *Palaeogeography, Palaeoclimatology, Palaeoecology* 278, 24-39.
- Montenat, C., Ott d'Estevou, P., Plaziat, J.C., Chapel, J., 1980. La signification des faunes marines contemporaines des évaporites messiniennes dans le Sud-Est de l'Espagne. Conséquences pour l'interprétation des conditions d'isolement de la Méditerranée occidentale. *Géologie Méditerranéenne* 7, 81-90.
- Omodeo Salé, S., Gennari, R., Lugli, S., Manzi, V., Roveri, M., 2012. Tectonic and climatic control on the Late Messinian sedimentary evolution of the Nijar Basin (Betic Cordillera, Southern Spain). *Basin Research* 24, 314-337.
- Ott d'Estevou, P., Montenat, C., 1990. Le bassin de Sorbas-Tabernas, in: Albert-de-Lapparent, I.G. (Ed.), *Les bassins Néogènes du domaine Betique Oriental (Espagne)*, pp. 101-128.
- Pagnier, H., 1976. Depth of deposition of Messinian selenitic gypsum in the Basin of Sorbas (SE Spain). *Mem. Soc. Geol. It.* 16, 363-367.
- Pedraza, A., Galindo-Zaldívar, J., Tello, A., Marín-Lechado, C., 2010. Intramontane basin development related to contractional and extensional structure interaction at the termination of a major sinistral fault: The Huércal-Overa Basin (Eastern Betic Cordillera). *Journal of Geodynamics* 49, 271-286.
- Platt, J.P., Allerton, S., Kirker, A.I., Mandeville, C., Mayfield, A., Platzman, E., Rimi, A., 2003. The ultimate arc: Differential displacement, oroclinal bending, and vertical axis rotation in the External Betic-Rif arc. *Tectonics* 22, 1017.
- Riding, R., Braga, J.C., Martín, J.M., 1991. Oolite stromatolites and thrombolites, Miocene, Spain: analogues of Recent giant Bahamian examples. *Sedimentary Geology* 71, 121-127.
- Riding, R., Braga, J.C., Martín, J.M., Sánchez-Almazo, I.M., 1998. Mediterranean Messinian Salinity Crisis: constraints from a coeval marginal basin, Sorbas, southeastern Spain. *Marine Geology* 146, 1-20.
- Riding, R., Braga, J.C., Martín, J.M., 1999. Late Miocene Mediterranean desiccation: topography and significance of the 'Salinity Crisis' erosion surface on-land in southeast Spain. *Sedimentary Geology* 123, 1-7.
- Riding, R., Braga, J.C., Martín, J.M., 2000. Late Miocene Mediterranean desiccation: topography and significance of the 'Salinity Crisis' erosion surface on-land in southeast Spain: Reply. *Sedimentary Geology* 133, 175-184.
- Roep, T.B., Dabrio, C.J., Fortuin, A.R., Polo, M.D., 1998. Late highstand patterns of shifting and stepping coastal barriers and washover-fans (late Messinian, Sorbas Basin, SE Spain). *Sedimentary Geology* 116, 27-56.

- Rouchy, J.M., Saint-Martin, J.P., 1992. Late Miocene events in the Mediterranean as recorded by carbonate-evaporite relations. *Geology* 20, 629-632.
- Roveri, M., Gennari, R., Lugli, S., Manzi, V., 2009. The Terminal Carbonate Complex: the record of sea-level changes during the Messinian salinity crisis. *GeoActa* 8, 63-78.
- Saint-Martin, J.P., Néraudeau, D., Lauriat-Rage, A., Goubert, E., Secrétan, S., Babinot, J.F., Boukli-Hacene, S., Pouyet, S., Lacour, D., Pestrea, S., Conesa, G., 2000. La faune interstratifiée dans les gypses messiniens de Los Yesos (bassin de Sorbas, SE Espagne): implications. *Geobios* 33, 637-649.
- Sanz de Galdeano, C., Vera, J.A., 1992. Stratigraphic record and palaeogeographical context of the Neogene basins in the Betic Cordillera, Spain. *Basin Research* 4, 21-36.
- Sierro, J., Flores, A., J., Civis, J., González-Delgado, J.A., Francés, G., 1993. Late Miocene globorotaliid event-stratigraphy and biogeography in the NE-Atlantic and Mediterranean. *Marine Micropaleontology* 21, 143-167.
- Stokes, M., Mather, A.E., Harvey, A.M., 2002. Quantification of river-capture-induced base-level changes and landscape development, Sorbas Basin, SE Spain. *Geological Society, London, Special Publications* 191, 23-35.
- Stokes, M., 2008. Plio-Pleistocene drainage development in an inverted sedimentary basin: Vera basin, Betic Cordillera, SE Spain. *Geomorphology* 100, 198-211.
- Visser, R.L.M., Platt, J.P., van der Wal, D., 1995. Late orogenic extension of the Betic Cordillera and the Alboran Domain: A lithospheric view. *Tectonics* 14, 786-803.
- Weijermars, R., Roep, T.B., Van den Eeckhout, B., Postma, G., Kleverlaan, K., 1985. Uplift history of a Betic fold nappe inferred from Neogene-Quaternary sedimentation and tectonics (in the Sierra Alhamilla and Almeria, Sorbas and Tabernas Basins of the Betic Cordilleras, SE Spain). *Geol. Mijnb.* 64, 397-411.
- Wu Qiang, Xu Hua and Zou Xukai, 2005. An effective method for 3D geological modeling with multisource data integration. *Computers and Geosciences*, v.31, p.35-43.

Figures captions:

Fig. 1: Simplified structural map of Southeastern Spain with location of the main metamorphic domes of the Sierra de los Filabres-Nevada and the Sierra Alhamilla-Cabrera and the main sedimentary basins.

Fig. 2: Geology and stratigraphy of the Sorbas Basin area. (A). Synthetic stratigraphic log of the sedimentary series within the basin. (B). Geological map of the Sorbas Basin modified after Ott d'Estevou and Montenat (1990), García Monzón *et al.*, (1974) and own field observations Projection UTM Zone 30 (WGS84 ellipsoid). XY transect represents the location of the synthetic cross-section displayed in C; Background is displayed a slope picture from the Digital Elevation Model of the basin. (C). N-S synthetic cross-section of the basin showing the asymmetrical structure of the deposits. Note the onlap progradation of post-Tortonian deposits, to the North, on top of the metamorphic rock units of the *sierra*. The inset details the geometry of the Messinian Erosional Surface in the Moras area. See location of the cross-section XY in the geological map.

Fig. 3: Compilation of (1) our observation sites (red dots), (2) most relevant bedding measurements that we performed in the Sorbas Basin and (3) existing measurements from the literature (black diamond) used for 3D modelling of the shallow structure of the basin. Background is displayed a slope picture from the Digital Elevation Model of the basin.

Fig. 4: (A) N-S synthetic cross-section running from the Zorreras hill (Fig. 2 for location), to the north, to the Barranco del Infierno folded area to the south. Spatial relationships between latest Messinian-earliest Zanclean deltaic deposits and Messinian evaporitic ones can be observed (see legend in Figure 2). Note, in particular, the progressive northward pinch out of the Messinian gypsum. The Sorbas calcarenite is laterally equivalent to the bottomset beds of the Gilbert-type fan deltas and deposited in a

shallow, lagoonal to coastal, environment (Roep *et al.*, 1998). This latter is located in the tectonically uplifted southern margin of the basin. (B) Southward thinning of the Zorreras (Pliocene topset beds of the Gilbert-type fan deltas) over the lagoonal calcarenite of the Sorbas Member as observed along the N340 road crossing the Sorbas City.

Fig. 5: (A) Uninterpreted and (B) interpreted panoramic view of the Barranco del Infierno section showing the northward thinning of the Messinian gypsum beneath the Pliocene platform deposit. (C) Messinian gypsum beds showing an eroded upper surface covered by post-MSC marine sediments and its synthetic log. (D) Reddish ferruginous crust developed above the erosive contact between the Yesares Messinian gypsum and the Sorbas Member.

Fig. 6: Morphology of the folded post-evaporitic coastal sandstone (Sorbas Member) over the evaporitic formation. (A) Panorama showing two oblique fold axes. Note here the curved shape of the hinge lines. (B) Dome-shape folding highlighted through the geometry of the bedding intersection with topography. Hilly relief of the area is partly controlled by the anticline location. (C) Location of cross-sections.

Fig. 7: (A) Very tight synform separating two dome shape folds in the western Barranco del Infierno area. The two orientation measurements are of normal series beddings. (B) The syn-kinematic accommodation space created into the syncline is filled by continental conglomerate belonging to the Zorreras Member. See location in Figure 6.

Fig. 8: Comparison between the structures computed from the shallow 3D model and the field-based geological map. The synthetic log used for the 3D modeling (A) shows the main stratigraphic relationships between each geological unit based on field observations and the synthetic log of the area (see Figure 2A). Such a pile is used to give a sequence ordering of geological units's interpolation during computation. The geological map of the modeled area (B) is comparable to the field-based one (C) showing that the shallow geometry of the basin has well been taken into account. Black arrows point out the major unconformities reproduced in the model and red points mark all observation sites, with structural and/or sedimentary data, used for modeling. Note that Quaternary sediments, white colored on the left-side geological map, are not considered for modeling. The area enlarged in boxes (D) and (E) displays the same local erosion features along the Río Aguas River and its tributaries, in particular along the Barranco del Infierno and Barranco del Hueli.

Fig. 9: Comparison between (A, B) field observations made at Cortijo de Hoyo, revealing the erosion separating marine post-MSC deltaic sediments and the Messinian gypsums, and (C) the same cross-section extracted in the 3D model showing the relatively low dipping morphology of the MES. Location on Figure 8D, E.

Fig. 10: Outputs from the shallow 3D model of the basin. (A) 3D representation of the Messinian Erosional Surface in the Sorbas Basin, showing southward fluvial incisions of the Góchar, Moras and Cariatiz areas, currently filled by the submarine part of Gilbert-type fan deltas. (B) Map of the thickness of the gypsums preserved from late erosion, in the Sorbas Basin, plotted over the geological map. The red line represents the predicted extension of the gypsum before the major erosion. Red arrows indicate possible trajectories of fluvial system developed during the peak of the Messinian Salinity Crisis.

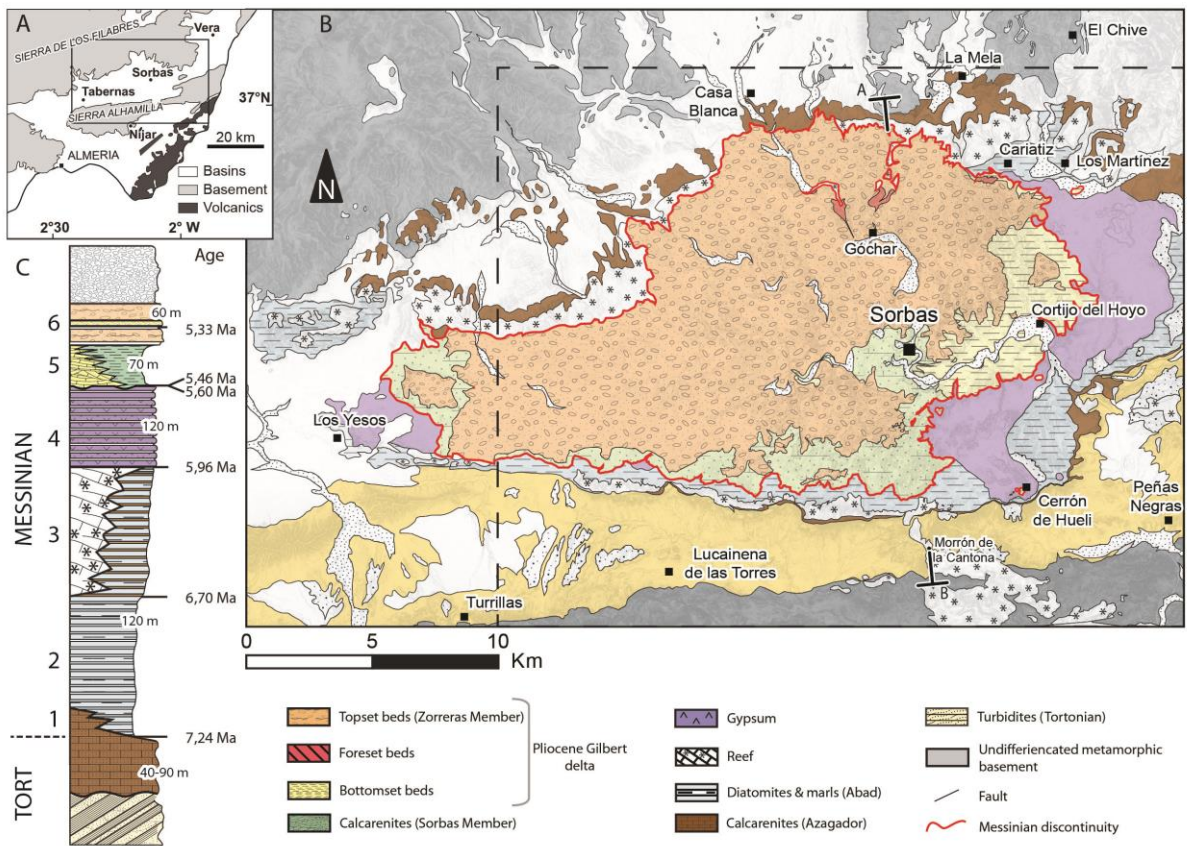
Fig. 11: (A) Spatial distribution and (B) stereographic projection of bedding measurements used in the high-resolution 3D model (see location in Figure 3).

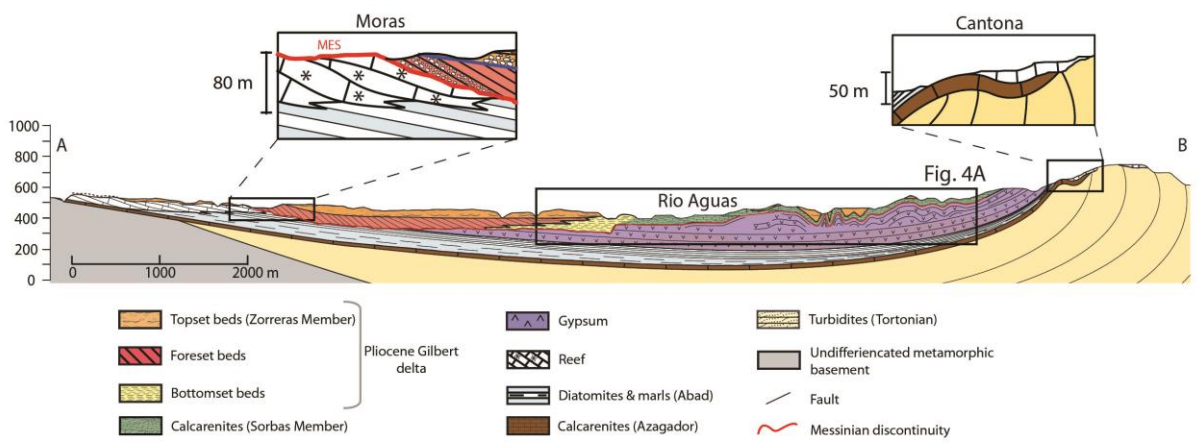
Fig. 12: A, B. Oblique 3D views of the Barranco del Infierno model displaying the predicted geometry of the Sorbas Unit above the gypsum. C. 3D view of the interpolated basal surface of the Sorbas Unit showing a strongly folded structure with dome shapes. D.

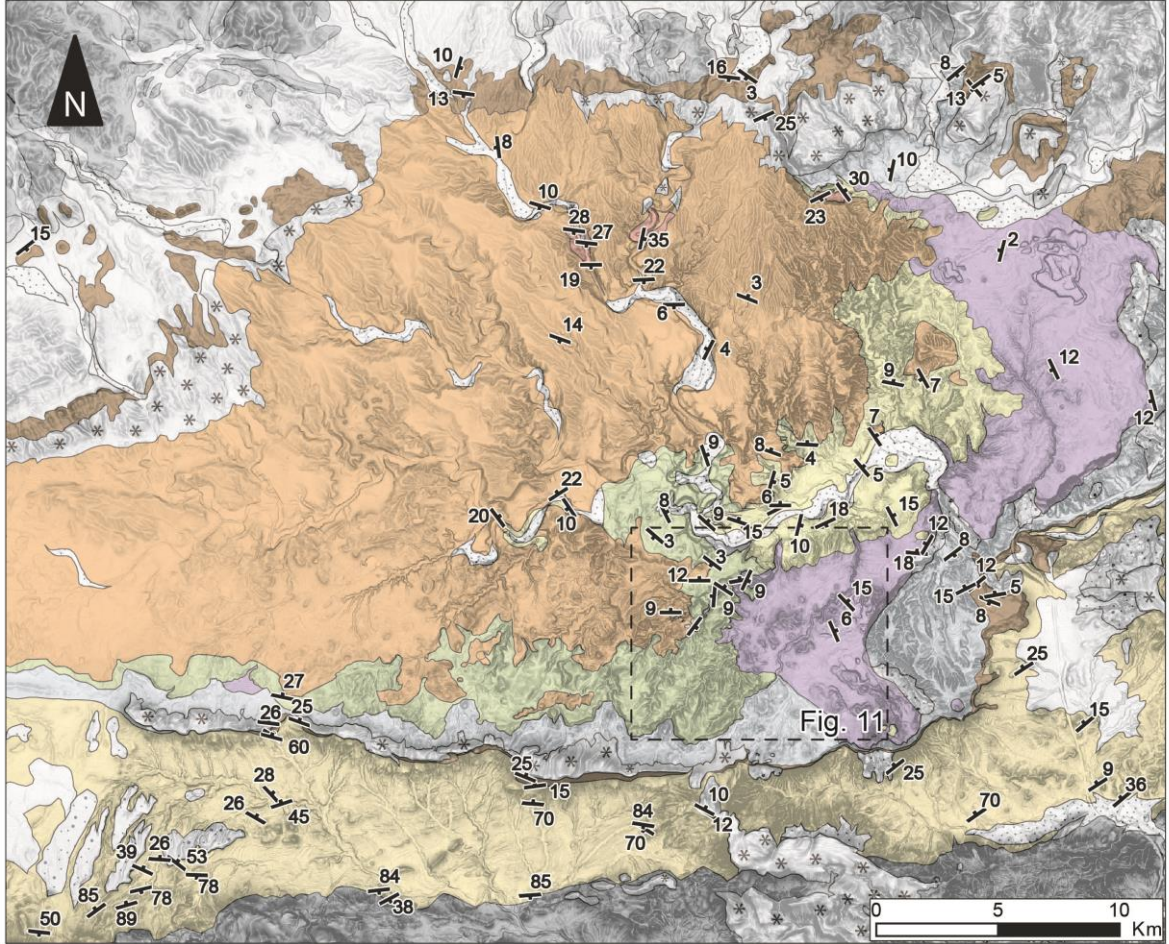
Contour map of the elevation of the interpolated basal surface of the Sorbas Unit. C and D: white areas correspond to valleys where gypsum is outcropping below the Sorbas Unit.

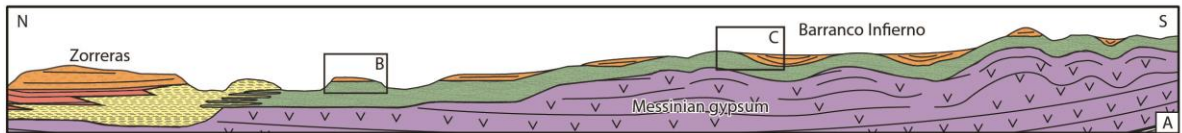
Fig. 13: Intersection of horizontal planes (450, 425 and 400 m high) with the interpolated bedding envelope surfaces. The Sorbas Member is displayed in green with lighter colours corresponding to younger layers into the formation. Gypsum is displayed in purple and the MES as a red line. In each map, the “bedding trajectories” show a very good consistency with the bedding measurements made for the corresponding altitude (~450, ~425 and ~400 m height).

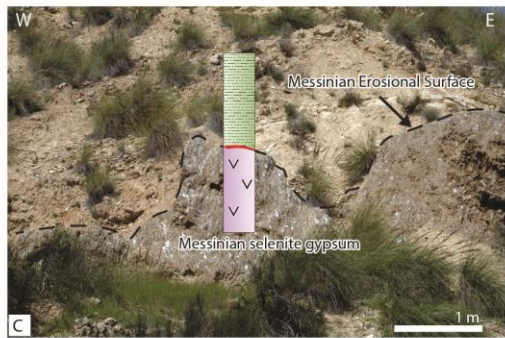
Fig. 14: Cross-sections of the interpolated sedimentary layers of the area. Gypsum is displayed in purple and the Sorbas Member in green. Bedding orientation measurements are projected from a distance of maximum 100 m from each side of the sections with apparent dips represented. A-B strikes N105, C-D strikes N95 and E-F strikes N180 (see location in Fig. 11 and 12). Despite their contrasted orientations, cross sections display similar folding of the Sorbas Member with wavelength of 250 to about 350 m above the gypsum.





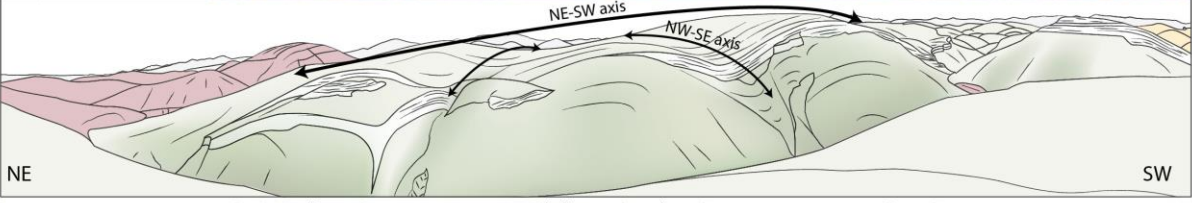








A Cross-section 1



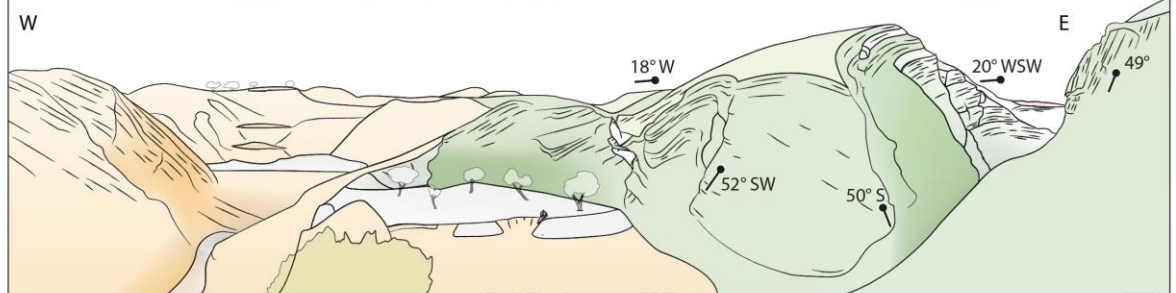
Continental formation
 Zorreras member

Shallow marine calcarenite
 Sorbas member

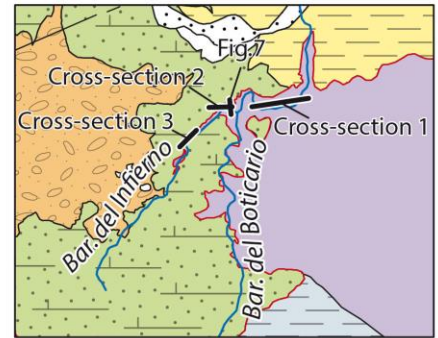
Evaporite - gypsum
 Yesares member

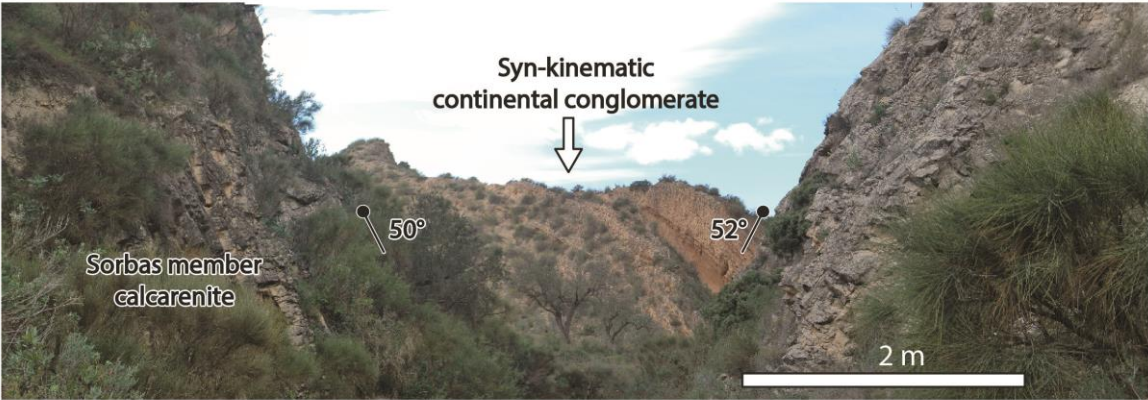


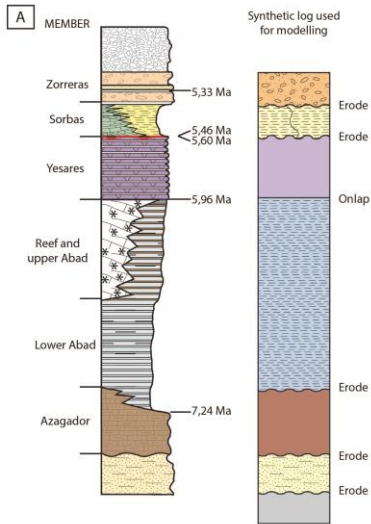
B Cross-section 2



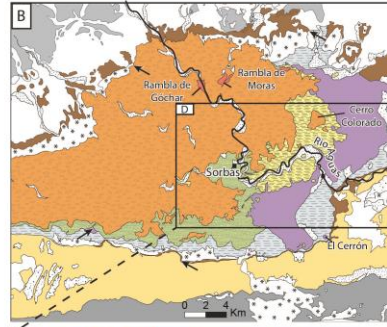
C Cross-section 3



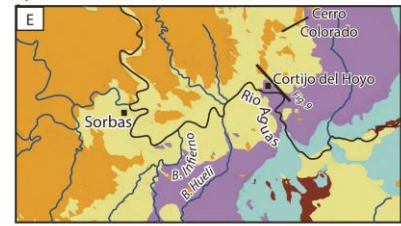
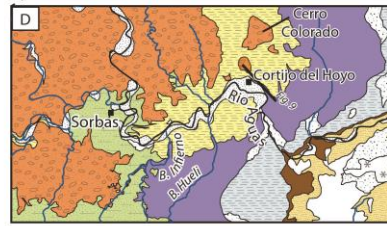
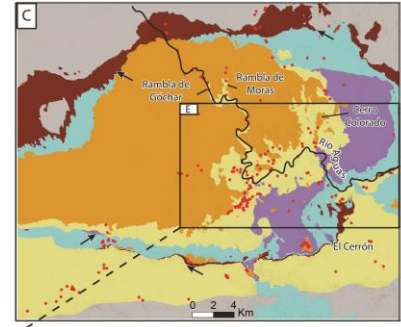


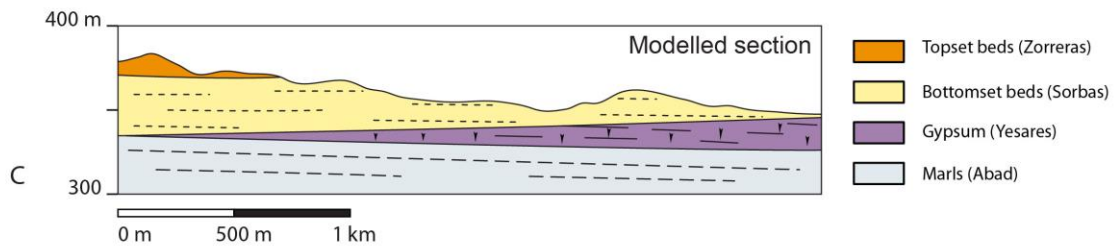
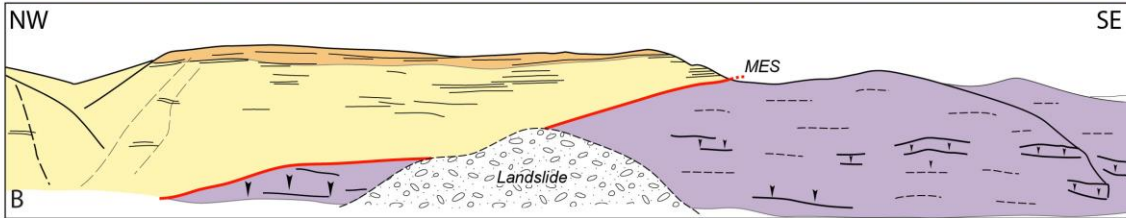


Geological data

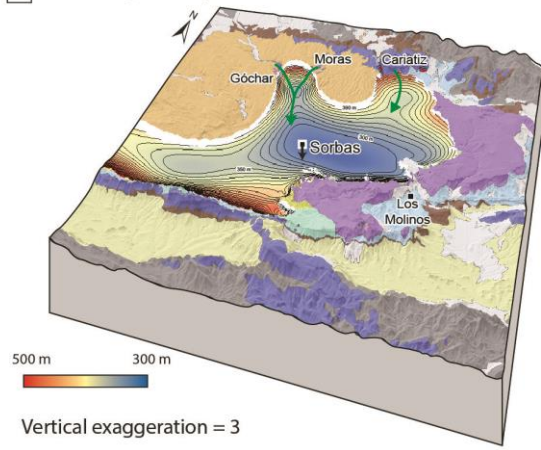


Modeled geological outlines

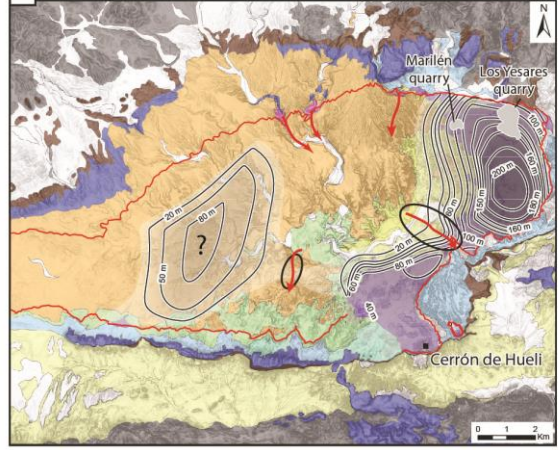


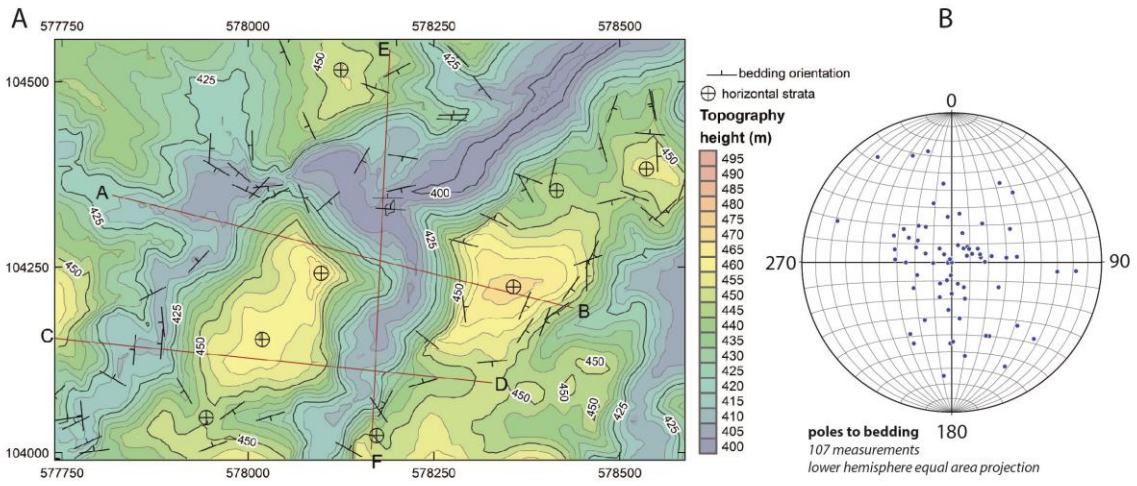


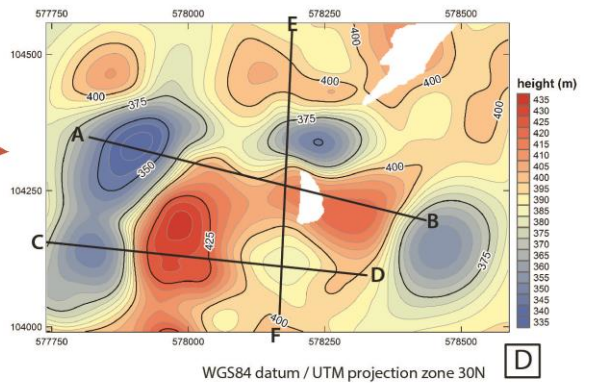
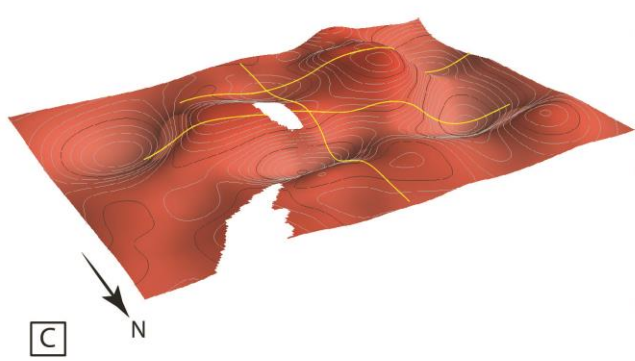
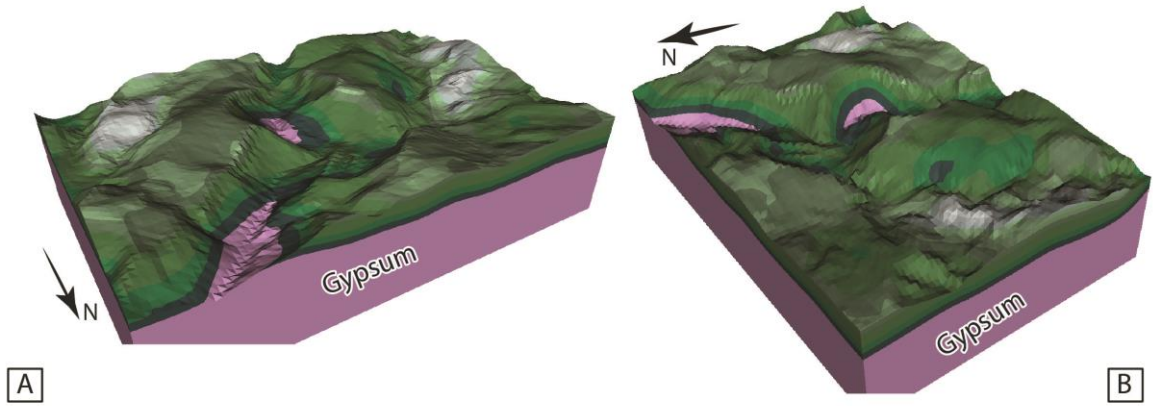
A Modeled geometry of the MES



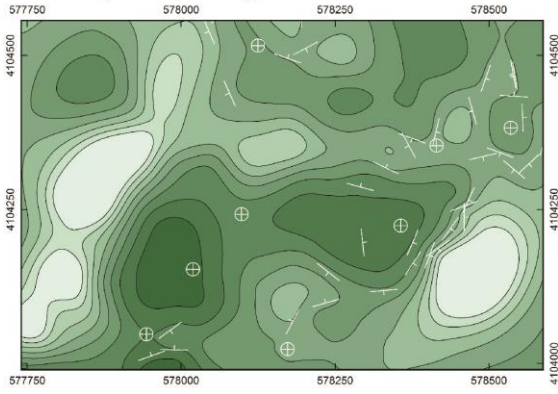
B Predicted thickness of the remaining gypsum



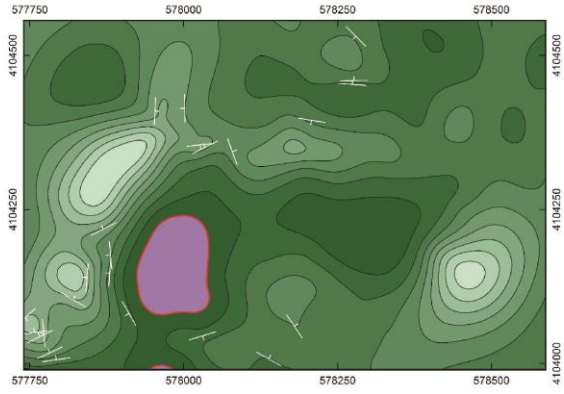




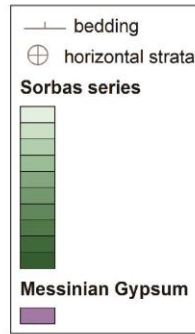
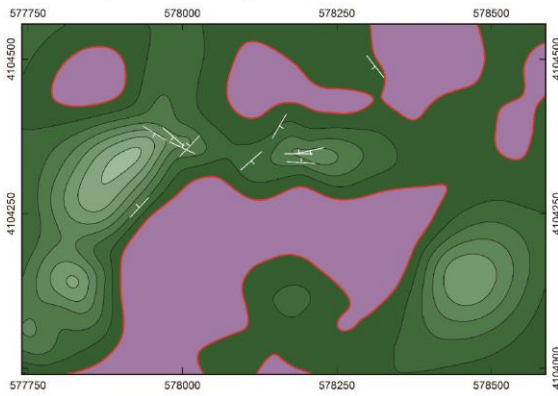
Horizontal plane at 450m height



Horizontal plane at 425m height



Horizontal plane at 400m height



WGS84 datum / UTM projection zone 30N

